Heart cockle shells transmit sunlight for photosynthesis using bundled fiber optic cables and condensing lenses

Dakota E. McCoy[1-3,*], Dale H. Burns[4], Elissa Klopfer[1], Liam K. Herndon[5], Babatunde Ogunlade[1], Jennifer A. Dionne[1,6,†], and Sönke Johnsen[3,†]

[1] Department of Materials Science and Engineering, Stanford University, Stanford, CA, USA
[2] Hopkins Marine Station, Stanford University, Pacific Grove, CA, USA
[3] Department of Biology, Duke University, Durham, NC, USA, 27708
[4] Department of Geological Sciences, Stanford University, Stanford, CA, USA
[5] Department of Chemical Engineering, Stanford University, Stanford, CA, USA
[6] Department of Radiology, Stanford University, Stanford, CA, USA

*Correspondence: Dakota E. McCoy, 496 Lomita Mall, Stanford, CA 94035; 724-766-4014; dakota.e.mccoy@gmail.com
[†] These authors contributed equally

Keywords
Photosymbiosis, *Symbiodinium*, photonics, optics, symbiosis, bivalves, *Corculum cardissa,* FDTD, FEM, transmission, transparency

Abstract:
Many animals convergently evolved photosynthetic symbioses, including two clades within the Bivalvia. Giant clams (Tridacninae) gape open to let light irradiate their symbionts, but heart cockles (Fraginae) can stay closed because sunlight passes through transparent windows in their shells. Here, we show that heart cockles (*Corculum cardissa* and *spp.*, Cardiidae) use intricate biophotonic adaptations to transmit more than 30% of visible sunlight (400-700nm) while transmitting only 12% of potentially harmful UV radiation (300-400nm). Beneath each window, microlenses condense light to penetrate more deeply into the symbiont-rich tissue. In the shell windows, aragonite forms narrow fibrous prisms that are optically co-oriented perpendicularly to the shell surface. These bundled “fiber optic cables" project images through the shell with a resolution of >100 lines / mm. Further, parameter sweeps in optical simulations show that the observed size (~1μm wide), morphology (long narrow fibers rather than typical aragonite plates), and orientation (along the c-axis) of the aragonite fibers transmit more light than many other possible morphologies. Heart cockle shell windows are thus: (i) the first instance of fiber optic cable bundles in an organism to our knowledge; (ii) a second evolution of condensing lenses for photosynthesis, as in plant epidermal cells; and (iii) a photonic system that efficiently transmits visible light while protecting photosymbionts from UV radiation. The animals’ soft tissues and the symbionts are therefore protected from predation and light stress.

Significance Statement

Photosymbiotic animals face a fundamental problem: they must irradiate their photosymbiotic symbionts without exposing their symbionts, or themselves, to predation and intense UV radiation. Reef-dwelling bivalves called heart cockles evolved an intricate biophotonic solution. Sunlight passes through clear windows in their shell, which are composed of aragonite fiber optic cable bundles and condensing lenses. This arrangement screens out UV radiation and allows the heart cockle to keep its shell closed. These intricate photonic adaptations are a novel solution to the evolutionary challenges of photosymbiosis: harnessing solar power while protecting against light stress and predation.

Introduction

Photosynthesis is the engine that powers much of life on our planet. Many researchers focus on photosynthesis in plants, algae, and cyanobacteria. However, animals also harness sunlight through symbiotic partnerships (1, 2). These animals– including reef-building corals, sponges, and bivalves--rely on a suite of optical adaptations to provide light for their photosymbionts (2). These optical adaptations are understudied, but have the potential to illuminate the coevolution of host and symbiont, the convergent evolution of photosynthetic systems, and the design of bio-inspired technologies.

Photosymbiotic bivalves are a particularly interesting group, despite receiving less attention than corals. Bivalvia is a class of primarily shelled molluscs that includes clams, oysters, mussels, and other marine and freshwater clades. Bivalves appear to have evolved obligate photosymbiosis twice, in two subfamilies within the family Cardiidae: the giant clams (Tridacninae) and the heart cockles (Fraginae (3–6); see (7) for review of other opportunistic symbioses in bivalves).

Bivalves in these two groups, having hard and normally opaque shells, had to evolve techniques to let light irradiate their soft tissues and the photosynthetic algae within. Giant clams solve this problem by gaping their shell open to bathe their mantle in downwelling sunlight. They further refined their photosynthetic capabilities through layered iridocytes that forward-scatter photosynthetically active radiation, back-reflect non-productive wavelengths, and absorb ultraviolet (UV) light that is then re-emitted at longer wavelengths (8–10). Certain cockles (e.g. *Clioniocardium nuttalli* and *Fragum spp.*) also temporarily gape their shells to expose mantle tissue, and, in some cases, extend mantle tissue out of and over the shell surface (7, 11). But there is an alternative solution that does not require that a clam expose its soft mantle to predation, UV radiation, and other dangers: windows in the shell.

Heart cockles (*Corculum cardissa* and *spp.*) evolved transparent windows in their otherwise opaque shell to allow light to reach their symbionts (12–16). The common name “heart cockle” typically refers to *Corculum cardissa*, but the genus *Corculum* contains seven recognized species– although *C. cardissa* is the only well-studied species from a biophotonics perspective (14, 17, 18). Here, we used the general term heart cockle to refer to the *Corculum spp.* shells studied herein.

Heart cockles have asymmetric shells (Figure S1), and are found partially buried in sand or corals, at depths of 0.5-10 meters (3, 13). Sunlight irradiates the photosynthetic dinoflagellates *Symbiodinium corculorum* within the mantle, gills, and foot (3, 12, 13). If placed in the shade, a heart cockle will move to the sun. If the sun-facing half of a heart cockle is covered with sand or mud, it will use its tiny foot to sweep its shell clean (16).

The shells of heart cockles are made from aragonite (19), a crystalline form of calcium carbonate ($CaCO_3$) widely used by aquatic invertebrates to make hard parts, and an organic matrix that directs the growth of the crystals (20). Two features distinguish the windows from the opaque regions of the shell. First, the aragonite within the windows forms elongated, fibrous, aragonite crystals (13–16, 21), the function of which has not yet been resolved (22). In opaque regions of the shell, the aragonite tends to be planar and crossed in orientation (termed "crossed lamellar" (15, 16)). Second, the windows are contiguous with transparent bumps on the inner surface of the shell that have been proposed to function as dispersing (23, 24) or condensing (15) lenses (13–16, 21).

Here, we apply a suite of photonic experiments and simulations to characterize the shell windows in heart cockles. We identify the optical properties of fibrous prismatic aragonite, scan and model the lenses beneath the windows, measure the spectrum of transmitted light, and conduct parameter sweeps to show whether these photonic adaptations sit at an evolutionary optimum.

Results and Discussion

Heart cockles have transparent windows that transmit sunlight and screen out UV radiation

Heart cockles (*Corculum cardissa* and *Corculum spp.*) are asymmetrical bivalves whose shells vary in shape and color (Figure S1). Some individual shells are strongly yellow (Figure S1A), orange-pink (Figure S1B), or pink (Figure S1D), while others are white with only hints of color (Figure AC,E). Heart cockles are antero-posteriorly flattened and form a heart-shaped outline when viewed from above (Figure S1A-E). The sun-facing side of heart cockle shells differs in profile from the sand-facing side, an asymmetry characteristic to heart cockles (Figure S1F). The sun-facing side is flat in some shells while other shells are shaped like a dome, dish, or combination of dome and dish (Figure S1F).

Transparent windows are arranged radially on the sun-facing half of the shell, with the exact shape and arrangement of the windows varying from triangular (Figure 1A) to radial stripes (Figure 1B) or even mosaics (Figure 1C). Using a lapidary saw, we cut flat 1 cm^2 fragments from heart cockle shell specimens; then, we suspended these fragments in seawater in a cuvette to measure transmission through the sun-facing side and the more opaque sand-facing side. The sun-facing side fragments included many tiny, evenly-spaced windows (Figure 1), so the 1 cm^2 fragments are a good representation of the overall shell.

The sun-facing side of the shell transmits substantial light to the symbionts within. We measured the spectral transmittance of the shell fragments in seawater using a UV-VIS spectrophotometer equipped with an integrating sphere to capture light transmitted at all angles. We showed that 16% to 40% of light (300-700 nm) penetrates the sun-facing side of the shell (average 27% transmission; Figure 1C; Figure 3A). In contrast, transmission through the sand-facing side was significantly lower, averaging 12% and ranging from 8.4% to 17% across shells (Figure 1, Figure 3A; two-sample t-test).

Further, the shell screens out UV radiation. Two to six times as much long-wavelength light penetrates the shell compared to short-wavelength light and UV radiation (300-400 nm vs. 600-700 nm) median ratio = 2.5, min = 1.9, max = 6.5), a significant difference (Figure 3B, two-

sample t-test). While the sand-facing side of the shell also screens out UV radiation, the sun-facing side of the shell does so to a significantly greater extent (Figure 3B; two-sample t-test). The sun facing side transmits a median of 31% of 400-700nm visible light (range = 17-47%), compared to only 12% of 300-400nm UV radiation (range = 8-20%). Giant clams, close relatives of the heart cockles and fellow photosymbionts, also screen or transform UV radiation through selective reflection as well as absorption and fluorescence re-emission (8–10).

We propose that the heart cockle's ability to screen out blue light and UV radiation may be a protective adaptation to resist DNA damage and reduce bleaching risk from high-energy UV radiation. The role of sunlight, and UV radiation, on the health of marine creatures is poorly understood but likely impactful (25–29).

Condensing lenses beneath each window focus sunlight

We found that some *C. cardissa* individuals have small transparent truncated bumps on the interior of their shells, located beneath each window; our simulations show that these bumps act as crude condensing lenses (Figure 2). To obtain the precise 3D surface morphology of these bumps without damaging the specimens (i.e., with no contact), we used a laser scanning microscope which applies confocal scanning, focus variation, and white light interferometry to obtain their 3D geometry. We centered the microscope on individual triangular windows (black arrow, Figure 2A) and produced a grayscale image encoding height information (Figure 2B). The triangular perimeters of each bump consistently matched the roughly triangular shape of the windows (see three sample bumps in Figure 2C-E), but bumps varied in diameter and height (Figure 2C-H). We imported the 3D morphology of the interior bumps (Figure 2C-F) into optical simulation software to test how the bumps affect light penetration into the soft tissues of the heart cockle (schematic in Figure 2I).

Our simulations demonstrate that the truncated lenses condense light with a large ~1mm depth of focus beginning around 500-750μm below the bump (Figure 2J-L). We propose that the bumps are an adaptation to help sunlight penetrate more deeply into symbiont-rich tissues (12). Many zooxanthellae are concentrated beneath the surface in the delicate, thin mantle tissue and gill filaments, suggesting that the lenses' depth of focus may correspond to symbiont location(12, 15). Previous researchers proposed that these bumps either disperse light over interior tissues (e.g., (23, 24)) or condense light into a beam that can penetrate deeper into the zooxanthellae-rich tissue (e.g., (15)). Our results support the hypothesis that the lenses condense light. Acetate peels from past work show that the aragonite microstructure within the bumps is a typical dissected crossed prismatic structure (rather than specialized fibrous prisms; see following paragraph (Carter & Schneider, 1997)).

Microlenses are widespread in nature as adaptations to manipulate light. Here, microlenses evolved for photosynthesis by the symbionts in heart cockles; shade-dwelling plants convergently evolved microlenses for photosynthesis through conical epidermal cells that concentrate sunlight (30). Heart cockle microlenses are made of aragonite; similarly, chiton molluscs use aragonite lenses for vision (31) while other marine creatures see or sense light with calcium carbonate lenses, for example, in light-sensitive brittlestar arms (32) and the schizochroal eyes of certain trilobites (33). Microlenses in nature can also produce richer colors by concentrating light onto pigments and reducing surface reflectance, as in the conical cells of flower petals (34–36) and super black color in peacock spiders (37).

Fiber optic cable bundles, composed of aragonite, form the microstructure of windows

In the shell windows, the mineral microstructure forms bundles of parallel natural fiber optic cables to transmit light (Figure 3). These “fibrous prismatic crystals” are elongate spires oriented roughly perpendicular to the shell surface (as revealed by SEM; Figure 3). As stated above, the shells of heart cockles (and many other marine invertebrates) are made from aragonite (19), a crystal form of calcium carbonate $CaCO_3$, inside an organic matrix of beta-chitin and other materials (20, 38, 39). In opaque regions of heart cockle shells, aragonite tends to be planar and crossed in orientation (termed “crossed lamellar”, either branching, complex, simple, or cone-complex (15, 16))-- a common morphology that makes shells harder to break but also opaque.

Further, aragonite is orthorhombic, and the aragonite fibers in heart cockle shell windows are co-oriented along the mineral’s c-axis (as revealed by FTIR; Supplemental Figure S3). The c-axis has the highest refractive index of aragonite’s three optical axes: 1.530 (a-axis), 1.681 (b-axis), and 1.686 (c-axis; (40)).

High-resolution images are visible through unpolished (Figure 3B-C) and polished (Figure 3D) fragments of shell windows. Unpolished windows transmit images at a resolution of 10 lines/mm (Figure 3B-C); polished windows transmit at 100 lines/mm (Figure 3D). Other researchers have observed these fibrous prismatic crystals of aragonite and debated whether or not they have a purpose, e.g., to act as fiber optic cables (13–16, 21, 22).

We show that the fibrous prismatic crystals act like parallel bundles of fiber optic cables in the shell windows– not just transmitting light but projecting high-resolution images through the window (Figure 3E-G). An image in focus through a microscope is out of focus when a polished fragment of shell window is placed on top of it (Figure 3E); when the microscope is refocused (Figure 3F) onto the top plane of the polished shell window, the object returns into focus (Figure 3G). We observed the same phenomenon when marking the top of a shell window with a permanent marker dot, which then appeared to be projected onto the opposite surface of the shell. Heart cockle shell windows are therefore analogous to ulexite (the “TV stone”), which is composed of self-cladding fiber optic crystals that transmit images through even fragments that are several cm thick (41, 42). Heart cockle shell windows project images at a higher resolution (~100 lines / mm; Figure 3D) than ulexite (~10lines/mm (41)), likely because the individual fibers are narrower.

To our knowledge, heart cockle shells are the first example of fiber optic cable bundles in a living creature. Indeed, fiber optic cables are themselves rare in nature. Deep-sea amphipods have crystalline cones which act as light guides via fiber optic principles (e.g., (43, 44)). *Phronima sp.* looks upward at downwelling light to catch prey; they have tapered cone cells about 1 mm long and up to 185 micrometers in diameter that guide and focus light to enable accurate vision in low-light conditions (43). The amphipod *Hyperia galba* has tapered cone cells about 300-600 μm long and 45-85 μm wide, with graded refractive indices to focus light and screen off-axis light– an arrangement which allows the amphipod to see while remaining transparent (44).

Beyond amphipod vision, two species of deep-sea sponge have glass spicules with fiber optical properties, although it is not known whether the sponges’ optical properties are useful to the animal or are a side effect of selection for mechanical rigidity. The Venus Flower Basket

sponge *Euplectella aspergillum* grows an intricate cage out of narrow spicules of amorphous, hydrated silica which can function as optical fibers and show remarkable mechanical strength compared to human-made glass (45–47). The large Antarctic sponge *Rossella racovitzae* has flexible spicules of amorphous hydrated silica that conduct light, even across a 90° bend, and– intriguingly– may support photosynthesis in shade-adapted diatoms that adhere to the spicules (48). These creatures tend to be found in the deep sea, although their ranges do extend into the photic zone; *Rossella racovitzae* lives at depths ranging from 18 to 2000m (49), while *Euplectella* lives at depths between 35 and 5000m (50–52).

Human-made fiber optic cables do not transmit all wavelengths of light with equal efficiency; low wavelength light scatters more due to imperfections and therefore is transmitted in lower proportions. The same phenomenon seems to occur in these natural fiber optic cable bundles, allowing heart cockles to screen out UV radiation using the fiber optic structure of their shell windows. The transmission spectra do not show noticeable absorption peaks, supporting the conclusion that UV radiation is screened primarily by imperfections in the fiber optic structures, rather than by absorbing pigments.

Computational parameter sweeps show that the fiber optic aragonite morphology, size, and orientation transmit more light than many other possible arrangements

We conducted a series of computational parameter sweeps to demonstrate that the observed morphology of the aragonite fibers transmits more light than many other possible morphologies. Specifically, we performed finite-difference time-domain and finite element method simulations using numerical optical solvers; we varied the morphology, size, and orientation of the fibers and extracted the transmittance from the simulations. The simulated fibers transmitted the most light when they matched our experimentally-observed morphology (consisting of fibrous prisms rather than lamellar planes; Figure 4A-B), size (width around 1 μm; Figure 4C), and orientation (along the c-axis; Figure 4 D-E).

Fibrous prisms of aragonite transmit more light than traditional planar, lamellar shapes (Figure 4A-C). Optical simulations demonstrate that the greater the proportion of fibrous prisms versus plates (Figure 4B-C), the greater the light transmission through the shell (Figure 4A). This mechanism of transparency through fiber-optics contrasts with another transparent bivalve, the window-pane oyster *Placuna placenta*. The window-pane oyster (used by some as a substitute for glass (53)), achieves transparency alongside mechanical strength through crystallographically co-oriented calcium carbonate plates oriented in parallel to the surface of the shell (54).

The ~1μm width of the observed fibers is superior to smaller fiber sizes for light transmission and only slightly inferior to all larger fiber diameters (Figure 4C). In its fibrous prismatic form, aragonite varies among marine bivalves in width (roughly, 0.5-5μm) and cross-sectional shape (researchers have observed rectangular, lath-type, rod-shaped, anvil-shaped, and irregular cross sections (55, 56)).

In shell windows, the aragonite fibers were oriented along their c-axis, the axis with the highest refractive index. Fiber optic cables transmit light through total internal reflection due to cladding with a material of a lower refractive index (57). Through a series of optical simulations, we showed that the c-axis orientation achieves significantly greater total light transmission compared to orienting along the lowest refractive index (Figure 4E-F; two-sample t-test), likely

due to the larger difference in refractive index between c-axis aragonite "core" (n_c=1.686) and the "cladding" (a- and b-axes, n_a=1.530, n_b=1.681, and organic matrix, n_{matrix}=1.435). Indeed, the "TV stone" ulexite is self-cladded by its own anisotropy, with the center being oriented along the highest of its three refractive indices (41) – just like the aragonite reported here.

By orienting its fibers along the highest refractive index, the aragonite maximizes the "self-cladding" contribution from its own refractive indices (41) --because light traveling at an angle will encounter lower refractive indices--as well maximizing the traditional cladding from the organic matrix. Here, natural selection acted upon an intrinsic feature of aragonite, anisotropy, to produce a biologically useful outcome: more transmitted light for photosynthesis.

Another marine animal exploits the anisotropy of aragonite for a different purpose, namely, vision. The chiton *Acanthopleura granulata* (Mollusca) lives on rocky substrates along seashores which are exposed to water during high tides and air during low tides; therefore, its eyes must be able to resolve images amidst background refractive indices of both air (n=1) and water (n=1.33). This chiton has aragonite lenses in its eyes which successfully focus light in both air and water thanks to the two different refractive indices of aragonite n_a=1.53 and $n_b \approx n_c \approx 1.68$ (31). Within the lenses, grains of aragonite are co-oriented along the c-axis (58).

Therefore, the observed morphology of shell windows seems to sit at a rough optimum for transmitting light. The shell is not entirely composed of windows, though, because transparency often compromises mechanical toughness in living creatures (58). Heart cockle shell windows are arranged in radial stripes, mosaics, or spots (Figure 1)– likely a balance between enhancing photosynthesis and avoiding shell-cracking predators. Chitons face the same tradeoff in their aragonite-lensed eyes; indeed, they have optimized for both mechanical toughness and optical function, in part by embedding the lenses– mechanically weak spots– within grooves to improve toughness (58).

Conclusion and Future Directions

In summary, heart cockles have evolved transparent windows in their shells with what is, to our knowledge, the first example of bundled fiber optic cables in a living creature. The aragonite fiber optics transmit light to the cockle's photosynthetic symbionts and, apparently as a side effect, project high-resolution images. Beneath each shell, condensing lenses focus sunlight to penetrate the symbiont-rich tissues. Together, the biophotonic arrangement screens out UV radiation, potentially protecting against the risk of bleaching or UV damage to DNA and other biomolecules. It would be worthwhile to compare the radiation spectrum experienced by symbionts in heart cockles to that of reef-building corals, and to examine the biological role of fluorescence across reef-dwelling creatures.

Beyond heart cockles and giant clams, bivalves may contain other potential models for understanding the evolution of photosymbioses. Researchers have observed opportunistic symbioses between photosynthetic algae and many other lineages of bivalves (7), including freshwater mussels *Anodonta cygnaea* and *Unio pictorum* (59), the clam *Fluviolanatus subtortus* (60), the scallop *Placopecten magellanicus* (61), the cockle *Clinocardium nuttallii (62, 63)*, and likely others (see (7) for comprehensive review). These "symbioses" (excluding the obligate symbioses in heart cockles and giant clams) are not known to be mutually beneficial and, indeed, may be parasitic (22). One indirect measure of mutualism, rather than parasitism,

may be biophotonic adaptations in the host to maximize light transfer and screen out UV radiation (as we see in the heart cockles).

The heart cockles' fiber optic cables and microlenses may inspire optical technologies. Previously, the glass spicules of sponges inspired lightweight mechanical architectures (64), while microlenses in peacock spiders inspired antireflective polymer microarrays (65).

Acknowledgements and Funding

DEM is supported by the Stanford Science Fellowship and the NSF Postdoctoral Research Fellowships in Biology PRFB Program, grant 2109465.

Figures

Figure 1: Transparent windows in heart cockle shells transmit 16-40% of sunlight and significantly screen out UV radiation.

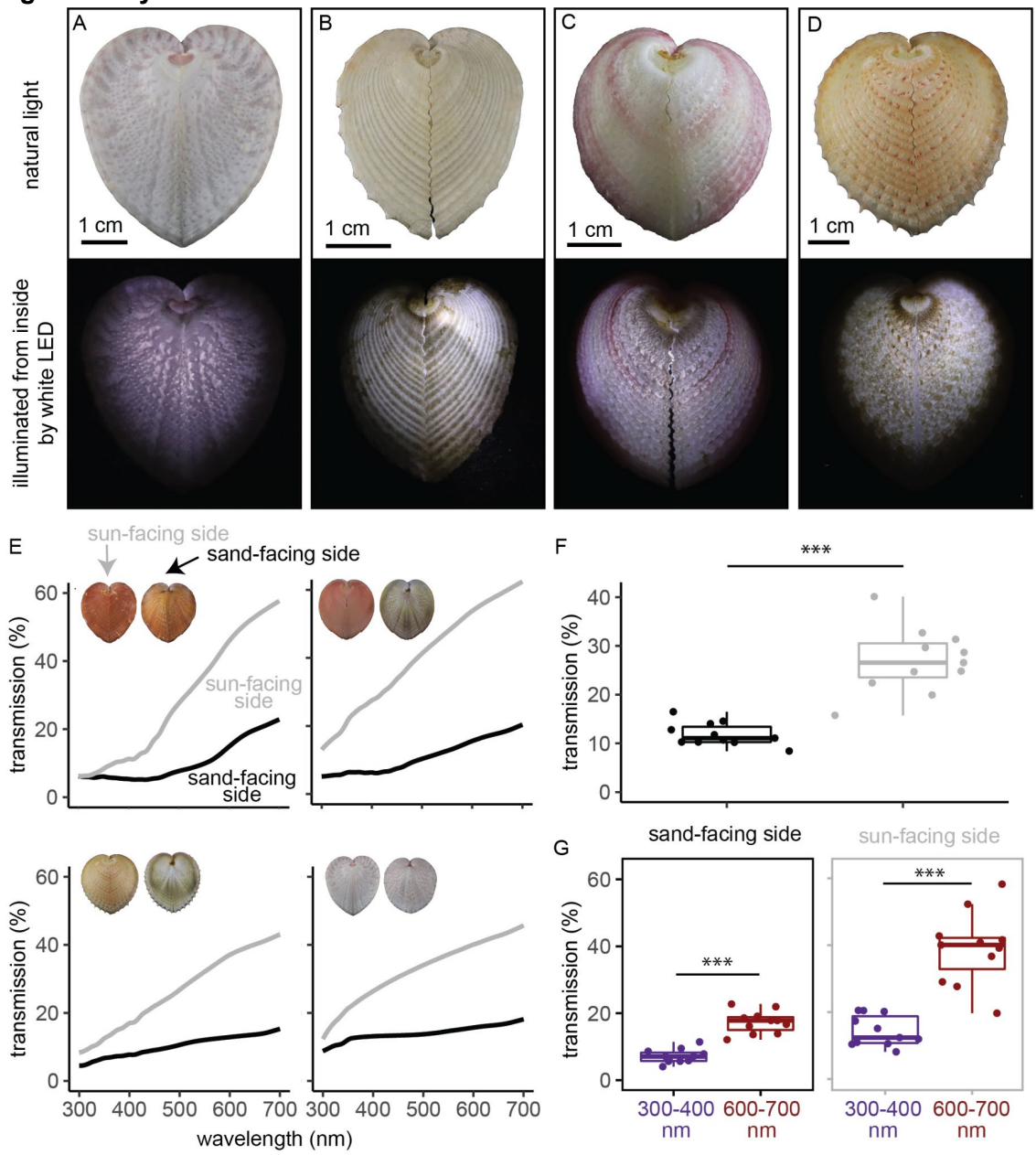

Figure 1: Transparent windows in heart cockle shells transmit 16-40% of sunlight and significantly screen out UV radiation. (A-D) We placed white LED lights inside the shell to demonstrate light transmission through the windows on the sun-facing side of the shell. The top row has natural light images of the sun-facing sides of four shells; the bottom row has images of the same side of the shells lit up from inside by a single white LED bulb. (A) *Corculum lorenzi*; (B-D) *Corculum cardissa.* **(E)** Shells show transmission spectra that vary in shape by shell color and rise at higher wavelengths, more dramatically for the sun-facing side (black curve) than the sand-facing side (grey curve). Here we plot four sample transmission curves for three *Corculum*

cardissa shells and one *Corculum lorenzi* (bottom right); see Supplemental Figure S2 for full transmission results. The inset images show the sun-facing side (left) and sand-facing side (right) of each shell in natural lighting. **(F)** The sun-facing side of the shell transmits 16% to 40% of sunlight (median = 27%), while the sand-facing side transits 8% to 17% of sunlight (median 11%), a significant difference (two-sample paired t-test, total transmission; p=<0.0005., 95% CI = [11, 19.2], mean diff. = 15.1, degrees of freedom = 10). **(G)** Shells transmit significantly more long-wavelength red light (600-700 nm) than short-wavelength UV and blue light (300-400 nm), particularly on the sun-facing side (sun-facing side; p<0.0005, 95% CI = [17.7, 31.4], mean diff. = 24.5, degrees of freedom = 10; sand-facing side: p<0.0005, 95% CI=[7.85, 12.4], mean diff. = 10.1, degrees of freedom = 10). The sun-facing side screens out UV light to a significantly greater extent than does the sand-facing side (p=0.00035, 95% CI=[8.34, 20.5], mean diff. = 14.4, degrees of freedom = 10).

Figure 2: Condensing lenses with truncated caps underneath the windows focus sunlight.

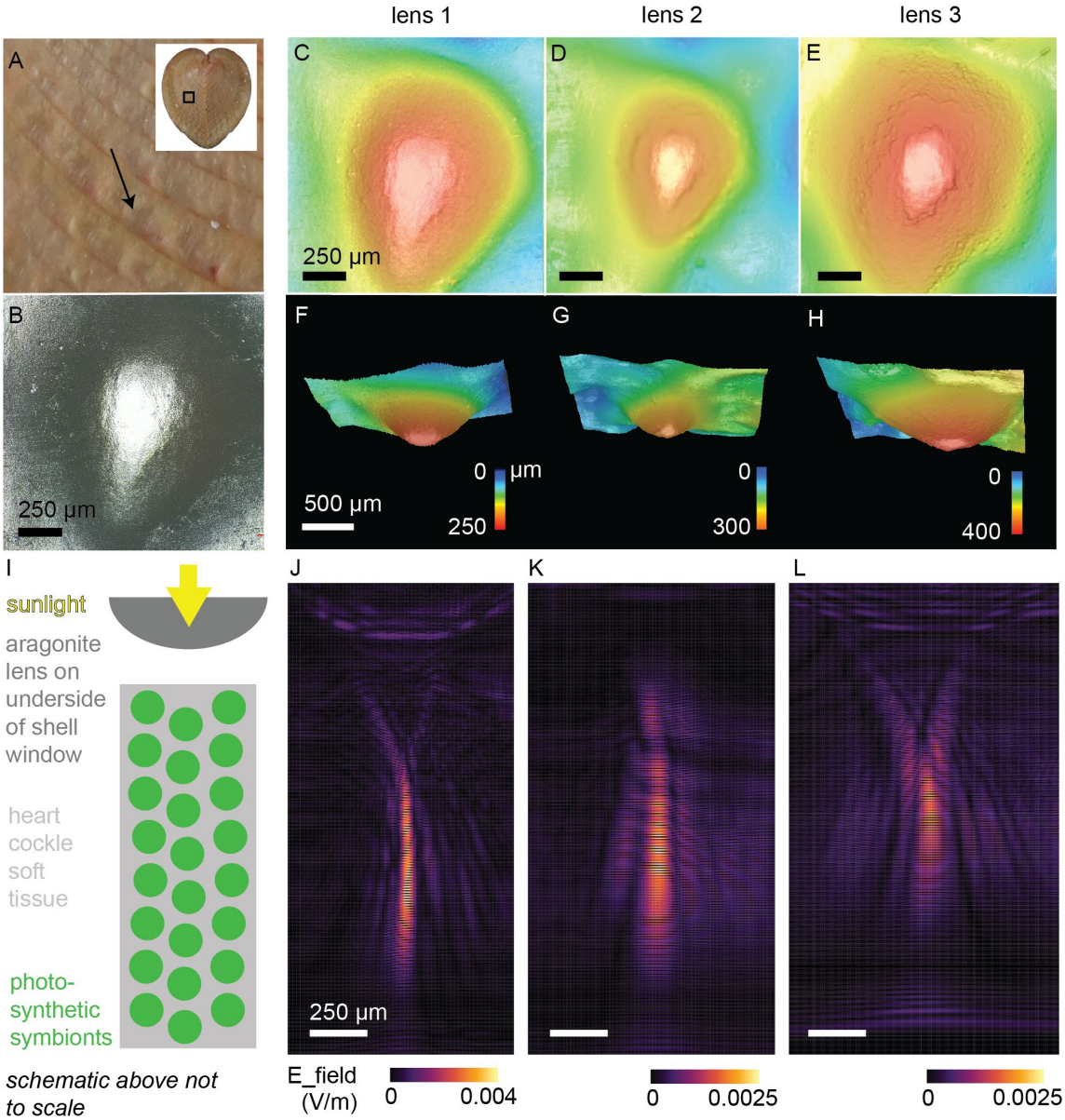

Figure 2: Condensing lenses with truncated caps under the windows focus sunlight. By "truncated", we refer to the flattened tips of the lens. **(A)** Shell windows are often triangular in shape (black arrow). **(B)** Beneath each shell window in some shells, the aragonite forms a lens shape roughly 750 µm in diameter. The exact size and shape of the lens varies from shell to shell. **(C-D)** 3D image of a single lens, showing truncated top. **(E-G)** 3D images of two more lenses, showing truncated top and variation in size and shape. **(H-I)** We imported the 3D scans in (C-G) into finite-difference time-domain (FDTD) optical simulation software to demonstrate that the lens focuses sunlight into a parallel beam. The input light geometry is a broadband (400-700 nm) plane wave. The wavelength of light pictured in J-L is 509 nm; results are similar across wavelengths.

Figure 3: Shell windows use natural fiber optics to project images with very high resolution (100 lines/mm).

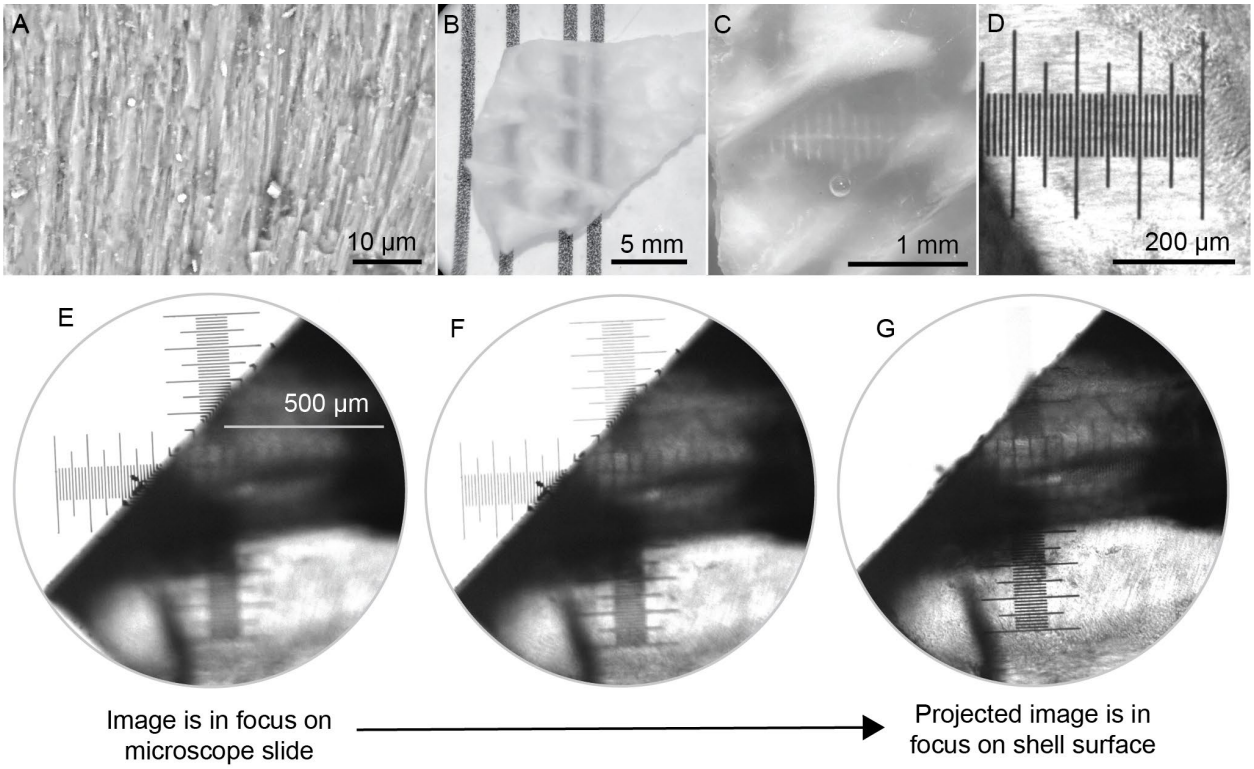

Figure 3: Shell windows use natural fiber optics to project images with very high resolution (100 lines/mm). (A) A cross-sectional SEM of a single shell window shows fibrous prisms of aragonite oriented roughly perpendicularly to the shell surface (the "fibrous prismatic layer"). These prisms act like fiber optic cables. In **(B-G),** we placed a small 0.7mm thick fragment of shell from a heart cockle on top of a glass calibration slide with rulers of different resolutions to determine (i) the resolution at which images transmit and (ii) whether images merely are transmitted through the windows or are actually projected onto the surface of the shell. **(B)** A fragment of unpolished shell shows the contrast between windows (transparent regions) and the opaque surrounding shell (white regions). **(C)** Shell windows from an unpolished fragment transmit 10 lines / mm. **(D)** Shell windows from a polished fragment transmit 100 lines / mm. **(F-G)** Shell windows project images onto their surface (rather than merely transmitting images through). We focused the microscope on the ruler on a glass calibration slide, placed a polished piece of shell on top of the glass calibration slide, and then adjusted the focus to refocus on the surface of the shell (~0.7mm higher than the background glass slide). The image came into focus on the surface of the shell. In B-C, shell fragments were immersed in seawater.

Figure 4: The observed orientation, size, and shape of aragonite fibers allow them to transmit more sunlight than other alternatives.

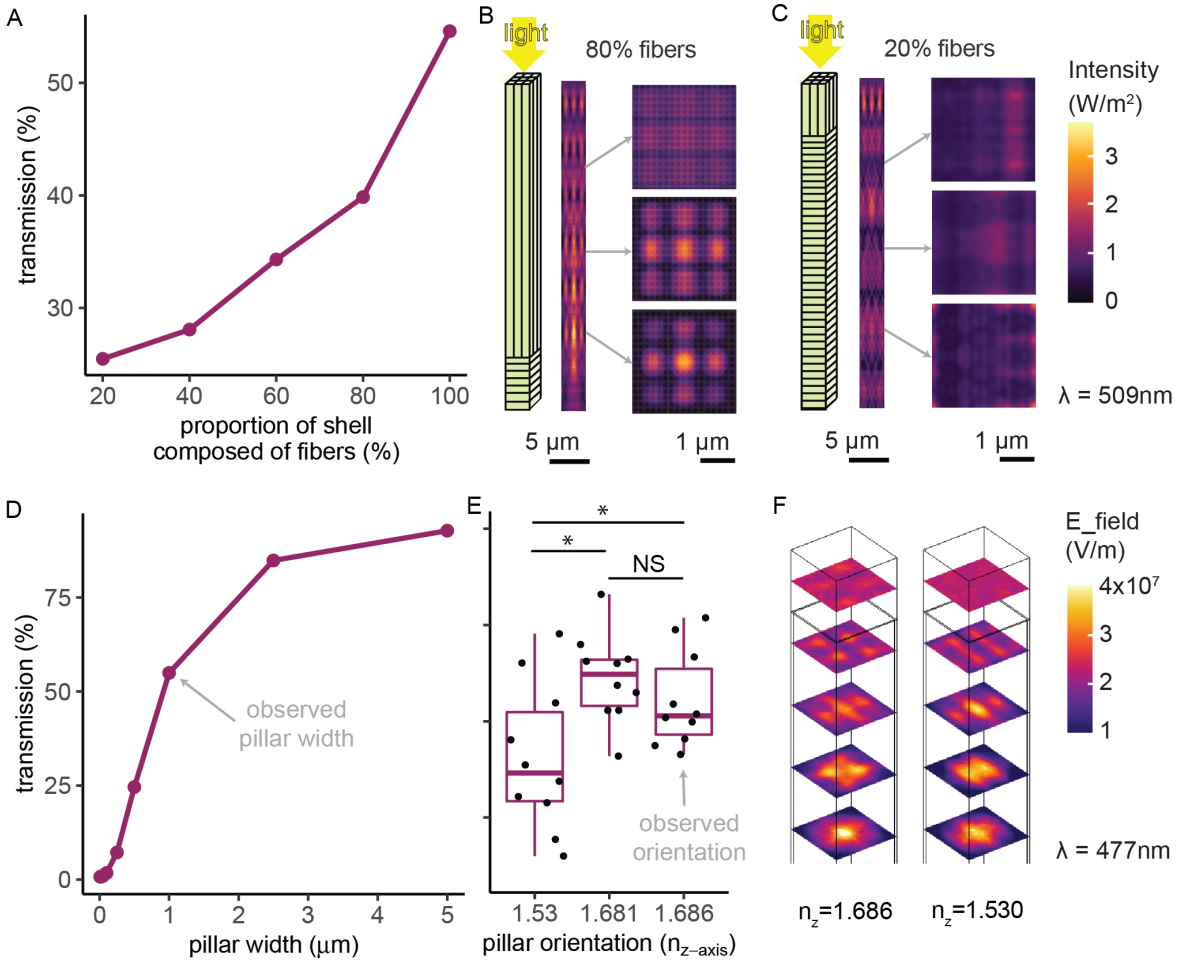

Figure 4: The observed orientation, size, and shape of the aragonite crystals allow them to transmit more sunlight than other alternatives. (A) More light is transmitted for shells with a higher proportion of fibers rather than planes (FDTD). **(B-C)** Light propagates differently through shells composed primarily of fiber-optic-cable shaped aragonite (left) compared to planar aragonite (right). We conducted FDTD simulations of a repeating element in the XY plane consisting of 3 x 3 fibers measuring 50µm in Z, and varied the proportion of the 50 µm stack that was composed of planar (rather than fibrous) aragonite. **(D)** Transmission increases proportionally with pillar width, such the observed pillar width-- 1µm – transmitted more light than narrower fibers and only a little less light than wider fibers. **(E)** Orientation along one of the two higher refractive indices (b or c), which is the arrangement we observed (Supplemental Figure S3), was associated with significantly greater light transmission compared to orientation along the a-axis (a-axis orientation vs. c-axis orientation: p=0.0015, 95% CI=[2.13, 7.78], mean diff. = 4.95, degrees of freedom = 21; a-axis orientation vs. b-axis orientation: (p=0.00065, 95% CI=[3.68, 11.7], mean diff. = 7.68, degrees of freedom = 21; b-axis orientation vs. c-axis orientation: no significant difference). **(F)** Screenshots of optical simulations illustrate how light propagates differently through a single pillar depending on the optical orientation (for both pillars, n_y=1.681; left, n_x =1.530; right, n_x =1.686). We conducted FDTD simulations in Ansys

Lumerical for (A-D) and FEM simulations in COMSOL for (E-F). For all panels, the refractive index of the organic matrix was set to n = 1.435 with imaginary component 0.001, and width of the organic matrix was set to 100nm; results were consistent when we varied the width and complex refractive index of the organic matrix (see Supplemental Figure S4).

Materials and Methods

Specimens

We obtained shells identified as members of the genus *Corculum* from the Yale Peabody Museum of Natural History (catalog numbers YPM108178, YPM108179, YPM108180, YPM108181) and from Jean Pierre Barbier, topseashells.com (catalog numbers, TS185203, TS163469, TS179955, TS177080, TS196641, TS179954, TS181027, TS164335, TS163836, TS196638, TS164403, TS196643). Because the shells are dry, the organic matrix within may not perfectly represent the organic matrix in living or recently collected shells.

Microscopy and Sample Preparation

To measure light transmission through the shells, we first cut 1 cm^2 fragments of each shell (one from the sun-facing side and one from the sand-facing side) using a Raytech Blazer four-inch lapidary saw. We suspended the shell fragments in seawater in cuvettes and used a Universal Measurement Spectrophotometer (UMS), Agilent Technologies Cary 7000 UV-VIS-NIR equipped with an integrating sphere to measure total percent light transmission. This method captures the most biologically relevant and realistic transmission, because it includes all angles of transmitted light, uses a fragment of actual shell including both windows and opaque regions, and measures light transmitted through the shell fragment suspended in seawater (therefore capturing the natural difference in refractive index between shell and medium). All measurements were normalized to a cuvette filled with seawater with no shell fragment.

To visualize light transmission through shell windows, we placed single LEDs on a wire inside closed shells.

To visualize image transmission through windows in an unpolished and polished shell fragment, we used a Leica DM4000 M light microscope. We placed the fragment in a dish atop a microscope calibration slide (which allowed us to identify the resolution of transmitted images). We obtained polished shell fragments by sending shell fragments to Brand Laser Optics (Newark, California, USA).

To gather surface microstructure information, we used a Keyence VK-X250/260K 3D Laser Scanning Confocal Microscope.

To obtain aragonite fiber structural information with minimal damage to the specimens, shell fragments were imaged using a JEOL JSM-IT500HR environmental scanning electron microscope. Prior to imaging, the fragments were coated with ~15 nm of amorphous carbon to ensure electrical conductivity on the specimen surface.

Raman and Fourier-Transform Infrared Spectroscopy

We confirmed that the shells, both windows and opaque regions, were composed of aragonite using Raman spectroscopy on the Horiba LabRAM HR Evolution Raman microscope and comparing the observed spectra to published literature ((19), DeCarlo 2018, La Pierre et. al 2014). The shells were illuminated with a 532 nm laser powered at ~11 mW with a 600 l/mm grating with ~1 cm^{-1} spectral resolution. Raman spectra were collected from 100 cm^{-1} to 1650 cm^{-1} using a 100x, 0.9 NA objective with a diffraction-limited spot size of ~1.5 μm and 15 second acquisition time.

To identify the crystallographic orientation of the aragonite in shell windows compared to opaque regions of the shell, we measured reflectivity using a Fourier transform infrared radiation spectroscopy (FTIR) setup. For these measurements, we collected the spectrum of infrared light (400 cm^{-1}-1800 cm^{-1}) reflected from shell windows using a Nicolet Continuum infrared microscope and a Nicolet iS50 FTIR spectrometer. These measurements were collected with 4 cm^{-1} resolution and an optical velocity of 1.8988 cm/s. The optical velocity is the speed at which the mirror moves in the interferometer when it scans through the Fourier-transformed spectrum (slower speeds give more accurate measurements). All results were averaged over 100 spectra. We used polished samples of shell that included both opaque and transparent regions, and we measured at three points: (i) transparent window, (ii) at the border between window and opaque, and (iii) opaque. By comparing the resulting spectra to published literature(66, 67), we were able to identify differences in crystallographic orientation between windows and opaque regions.

Optical Simulations

We performed optical simulations using both idealized and actual, imported microstructures. We performed finite-difference time-domain (FDTD) simulations in the software program Ansys Lumerical and finite element method (FEM) simulations in the software COMSOL.

To test whether the truncated lenses focused or dispersed light, we used FDTD simulations based on measured 3D morphological scans. To save computer memory, we imported 3D surface files (STL triangular surface files) with a scaling factor of 0.0001 (one-tenth the actual size of the lenses). We launched a plane wave normally incident (z-direction) on the lens, ranging in wavelength from 400 - 700 nm, and bounded the simulation on all sides by perfectly matched layers (PMLs). We placed frequency domain field monitors at regular intervals to identify the focal region of greatest intensity, then we centered XZ and YZ monitors on that focal spot.

To test the impact of aragonite being in a fibrous rather than lamellar/planar shape, we performed FDTD simulations of a 3 x 3 grid of fibers, each measuring 1 x 1 x 50 μm. For the aragonite fibrous prisms, we used the refractive index values of 1.530 (a-axis), 1.681 (b-axis), and 1.69 (c-axis). For the organic matrix, we chose a real refractive index of 1.43 following past work and varied the imaginary component over two values: 0.0001 and 0.001 (38, 39). We report the results for index 0.001 in the main text and the other in Supplemental Figure S4. Generally, molluscan shells are about 0.1-5% organic matrix by weight and the rest calcium carbonate (68); we varied the width of the organic matrix between pillars over three values: 100 nm, 50 nm, 25 (69). We report the results for organic matrix width 100 nm in the main text and the others in Supplemental Figure S4. For simulations incorporating layers of planar aragonite, we incorporated planes with thickness 1 μm in the Z direction and XY area spanning the entire XY plane of the simulation. The angle of the planes was randomly varied between 5 and 15 degrees (using the random() function). For these simulations, the simulation domain was bounded in the Z plane by perfectly matched layers and in the X and Y planes by periodic boundary conditions (to simulate an infinite array of fibers). We used a plane wave normally incident (z-direction), ranging in wavelength from 400 - 700 nm.

To test the impact of varying the size of the optical fibers, we repeated the above procedure but varied the pillar width over the following values: 10nm, 25nm, 50nm, 100nm, 500nm, 1μm, 2.5μm, and 5μm.

To test the impact of varying the optical orientation of the fibers, we performed finite element method (FEM) simulations in COMSOL on an idealized single fiber measuring 1 x 1 x 10 μm. We enabled Floquent boundary conditions in the X and Y planes to simulate the periodic nature of the aragonite fibers with ports above and below in the Z plane. We performed parameters sweeps to vary the X-axis, Y-axis, and Z-axis refractive indices over all six possible configurations (that is, we set n_x, n_y, and n_z equal to 1.686, 1.681, and 1.530 but systematically varied which axis had which index). In the results, we condense these six possibilities into the three different Z-axis possibilities. We swept over wavelengths from 485 nm to 725 nm by 20 nm, and here we report the total transmission through the bottom of the pillar.

For all simulations on idealized structures (aragonite fiber optic cables), we eliminated spurious resonances by changing the size of the modeled features over five values – 0.95, 0.975, 1, 1.025, and 1.05 times the actual size– and averaging the results (70). To make all simulations comparable, we adjusted the results to represent values for 200μm-high pillars. That is, for T= transmission(50μm-high pillars), we report T^4; to convert the transmission for 50μm to transmission for 200μm. For T= transmission(10μm-high pillars), we report T^{20}.

Supplemental Information

Supplemental Figure S1: Heart cockles (*Corculum spp.*) are asymmetrical, photosymbiotic bivalves.

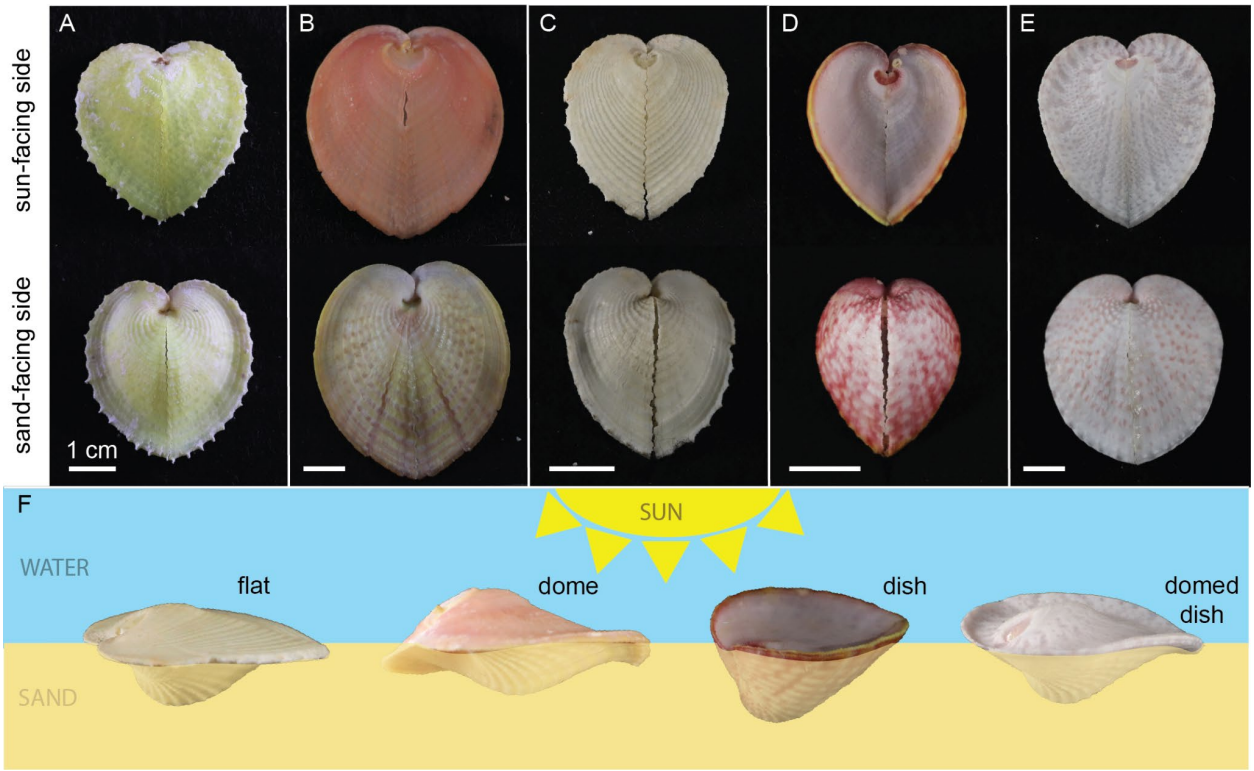

Figure S1: Heart cockles (*Corculum cardissa* and *Corculum spp.*) are asymmetrical, photosymbiotic bivalves. (A-E) Heart cockles come in many sizes, shapes, and colors across (A-C) *Corculum cardissa* and the seven other recognized species of *Corculum*, e.g., (D) *Corculum roseum* and (E) *Corculum lorenzi*. **(F)** The sun-facing side of heart cockle shells varies from a flattened, expanded pancake shake ("flat"; *Corculum cardissa*) to an arched dome ("dome"; *Corculum cardissa*) to a cup-shaped dish ("dish"; *Corculum roseum*) and combinations of these shapes (e.g., "domed dish"; *Corculum lorenzi*).

Supplemental Figure S2: Transparent windows allow the shell to transmit 16-40% of sunlight into the soft tissues.

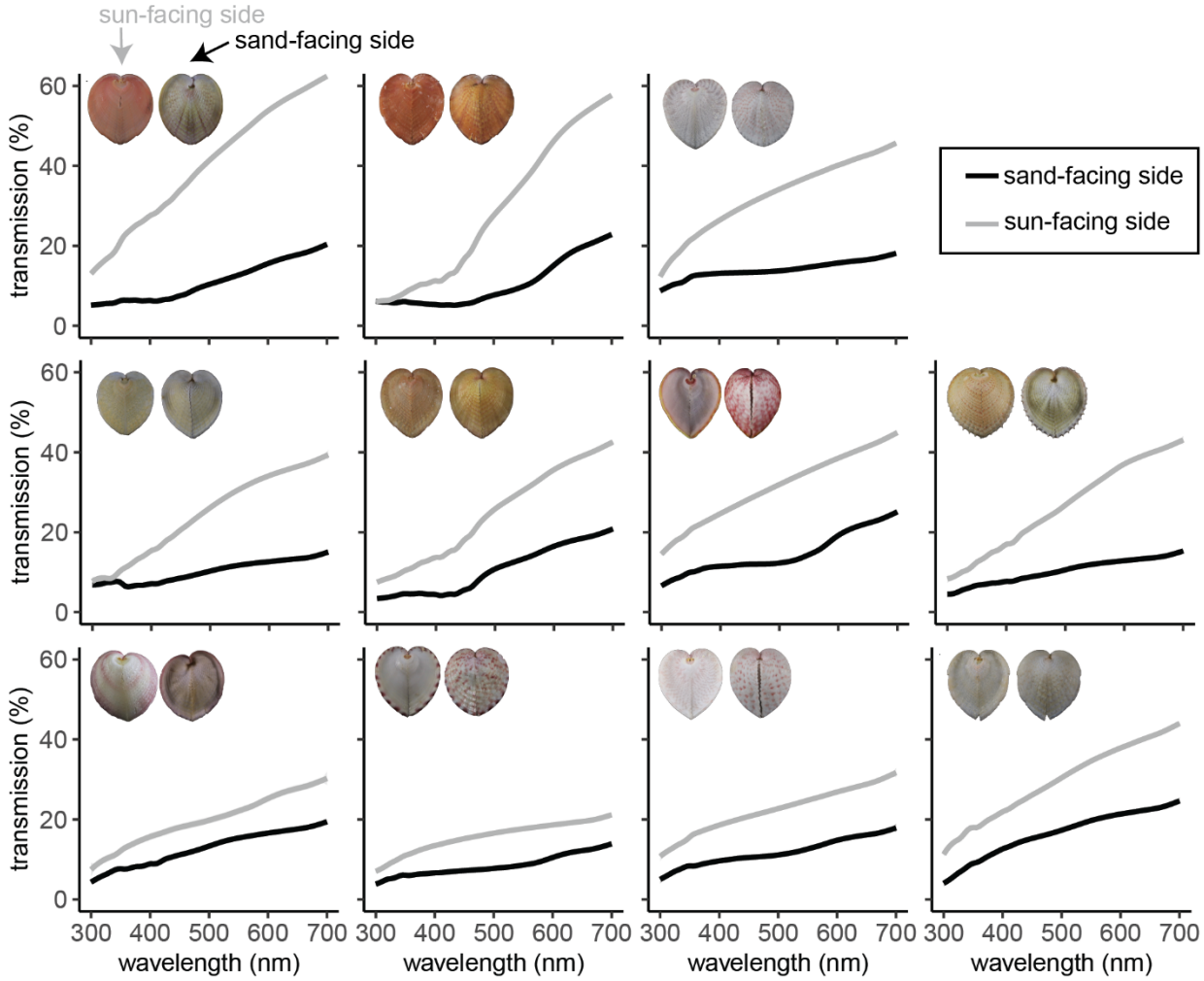

Supplemental Figure S2: Transparent windows transmit 16-40% of sunlight into the soft tissues. Grey lines indicate % transmission through the sun-facing (upper) half of the shell, and black lines indicate % transmission through the sand-facing (lower) half of the shell. For these measurements, a flat rectangular piece of shell approximately 1.5 cm by 1 cm was immersed in seawater. Each line represents three measurements, but error bars are small and concealed within the line width.

Supplemental Figure S3: FTIR demonstrates that shell windows have a high proportion of c-axis aligned aragonite crystals compared to opaque regions.

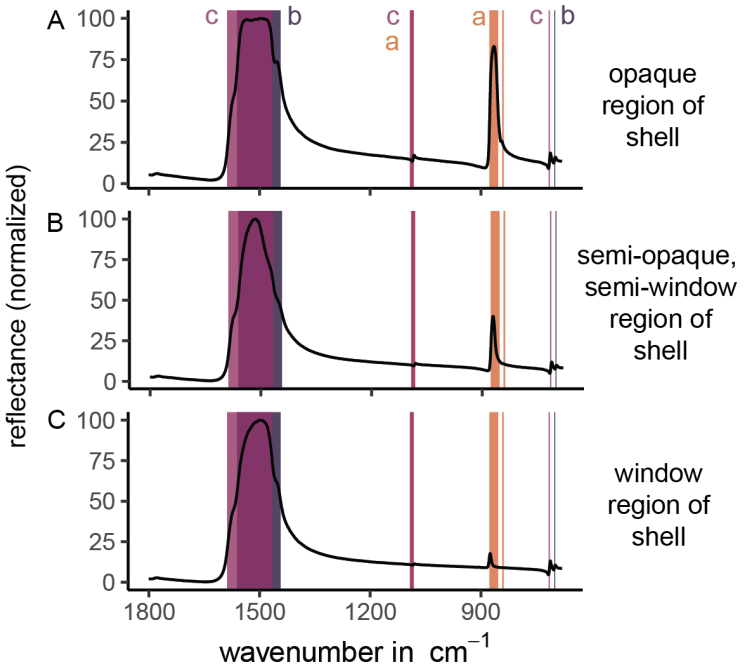

Supplemental Figure S3: FTIR demonstrates that shell windows have a high proportion of c-axis aligned aragonite crystals compared to opaque regions. Here we plot three characteristic spectra taken from polished fragments of shell. Peak location corresponds to crystallographic orientation (66, 67); a-orientation is highlighted in salmon, b-orientation in green, and c-orientation in yellow. B- and c-oriented crystals produce a very similar spectra, but the peak located between 853-877 cm -1 is unique to a. **(A)** Reflectance from an opaque region of the shell shows a high proportion of a-oriented crystals. **(B)** Reflectance from a semi-opaque, semi-window region of the shell shows a medium proportion of a-oriented crystals. **(C)** Reflectance from a window region of the shell shows a low proportion of a-oriented crystals. Because the c- and b- axes of aragonite are so similar, it is difficult to distinguish which of these higher refractive indices is oriented in the Z direction. According to the literature, the c-axis is generally thought to be parallel to the long axis of aragonite prisms (71); therefore, we make the same conclusion. Whether it is the c-axis, b-axis, or both, our results do not materially change.

Supplemental Figure S4: Sensitivity analyses show that results from simulations of the aragonite fiber optics are robust to variations in the refractive index and width of the organic matrix.

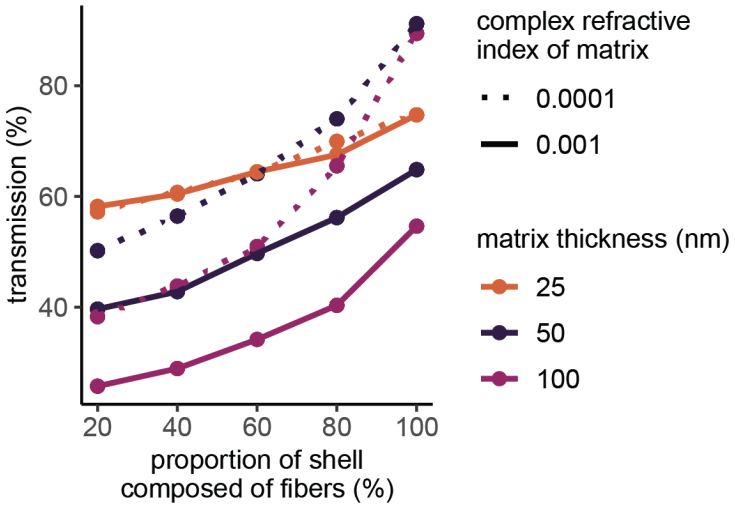

Supplemental Figure S4: Sensitivity analyses show that results from simulations of the aragonite fiber optics are robust to variations in the refractive index and width of the organic matrix. Here we plot the results of FDTD simulations where we varied the proportion of the shell that was composed of fibers (rather than planar aragonite), as in Figure 4A. The results are consistent across variations in the complex refractive index of the matrix and thickness of the matrix.

Bibliography

1. A. A. Venn, J. E. Loram, A. E. Douglas, Photosynthetic symbioses in animals. *J. Exp. Bot.* **59**, 1069–1080 (2008).

2. J. Melo Clavijo, A. Donath, J. Serôdio, G. Christa, Polymorphic adaptations in metazoans to establish and maintain photosymbioses. *Biol. Rev. Camb. Philos. Soc.* **93**, 2006–2020 (2018).

3. J. Li, *et al.*, Shedding light: a phylotranscriptomic perspective illuminates the origin of photosymbiosis in marine bivalves. *BMC Evol. Biol.* **20**, 50 (2020).

4. L. Kirkendale, Their day in the sun: molecular phylogenetics and origin of photosymbiosis in the “other”group of photosymbiotic marine bivalves (Cardiidae: Fraginae). *Biol. J. Linn. Soc. Lond.* **97**, 448–465 (2009).

5. J. Li, M. Volsteadt, L. Kirkendale, C. M. Cavanaugh, Characterizing Photosymbiosis Between Fraginae Bivalves and Symbiodinium Using Phylogenetics and Stable Isotopes. *Frontiers in Ecology and Evolution* **6** (2018).

6. S. Kawaguti, Heart shell Corculum cardissa (L.) and its zooxanthella. *Kagaku Nanyo*.

7. L. Kirkendale, G. Paulay, Treatise Online no 89: Part N, Revised, Volume 1, Chapter 9: Photosymbiosis in Bivalvia. *Treatise Online* (2017) https:/doi.org/10.17161/to.v0i0.6554.

8. A. L. Holt, S. Vahidinia, Y. L. Gagnon, D. E. Morse, A. M. Sweeney, Photosymbiotic giant clams are transformers of solar flux. *J. R. Soc. Interface* **11**, 20140678 (2014).

9. A. Ghoshal, E. Eck, M. Gordon, D. E. Morse, Wavelength-specific forward scattering of light by Bragg-reflective iridocytes in giant clams. *J. R. Soc. Interface* **13**, 20160285 (2016).

10. S. Rossbach, R. C. Subedi, T. K. Ng, B. S. Ooi, C. M. Duarte, Iridocytes mediate photonic cooperation between giant clams (Tridacninae) and their photosynthetic symbionts. *Frontiers in Marine Science* **7**, 465 (2020).

11. T. Ohno, T. Katoh, T. Yamasu, The origin of algal-bivalve photo-symbiosis. *Palaeontology* **38**, 1–22 (1995).

12. S. Kawaguti, Observations on the Heart Shell, Corculum. cardissa (L.), and Its Associated Zooxanthellae (1950).

13. M. A. Farmer, W. K. Fitt, R. K. Trench, Morphology of the symbiosis between Corculum cardissa (Mollusca: Bivalvia) and Symbiodinium corculorum (Dinophyceae). *Biol. Bull.* **200**, 336–343 (2001).

14. L. Kirkendale, J. J. ter Poorten, P. Middelfart, J. G. Carter, A NEW PHOTOSYMBIOTIC MARINE BIVALVE WITH WINDOW SHELL MICROSTRUCTURE (CARDIIDAE: FRAGINAE). *Phuket mar. biol. Cent. Res. Bull.* (2021) https:/doi.org/10.14456/pmbcrb.2021.9.

15. J. G. Carter, J. A. Schneider, Condensing lenses and shell microstructure in Corculum (Mollusca: Bivalvia). *J. Paleontol.* **71**, 56–61 (1997).

16. M. E. Watson, How a clam builds windows: shell microstructure in Corculum (Bivalvia: Cardiidae). *Veliger* **28**, 348–355 (1986).

17. ,MolluscaBase: Corculum. *World Register of Marine Species* (2022) (September 26, 2022).

18. G. T. Poppe, A listing of Philippine marine mollusks (2017).

19. J. D. Taylor, W. J. Kennedy, The shell structure and mineralogy of the Bivalvia. II. Lucinacea-Clavagellacea conclusions. *Bull. Br. Mus.* **22**, 253–294 (1973).

20. L. Addadi, D. Joester, F. Nudelman, S. Weiner, Mollusk shell formation: a source of new concepts for understanding biomineralization processes. *Chemistry* **12**, 980–987 (2006).

21. J. A. Schneider, J. G. Carter, Evolution and phylogenetic significance of cardioidean shell microstructure (Mollusca, Bivalvia). *J. Paleontol.* **75**, 607–643 (2001).

22. E. Savazzi, A review of symbiosis in the Bivalvia, with special attention to macrosymbiosis. *Paleontol. Res.* **5**, 55–73 (2001).

23. A. Seilacher, Fabricational Noise in Adaptive Morphology. *Syst. Biol.* **22**, 451–465 (1973).

24. A. Seilacher, Aberrations in bivalve evolution related to photo-and chemosymbiosis. *Hist. Biol.* **3**, 289–311 (1990).

25. B. E. Brown, R. P. Dunne, M. S. Goodson, A. E. Douglas, Bleaching patterns in reef corals. *Nature* **404**, 142–143 (2000).

26. V. R. Coelho, *et al.*, Shading as a mitigation tool for coral bleaching in three common Indo-Pacific species. *J. Exp. Mar. Bio. Ecol.* **497**, 152–163 (2017).

27. R. A. Kinzie, Effects of ambient levels of solar ultraviolet radiation on zooxanthellae and photosynthesis of the reef coral Montipora verrucosa. *Mar. Biol.* **116**, 319–327 (1993).

28. S. Anderson, *et al.*, Indicators of UV Exposure in Corals and Their Relevance to Global Climate Change and Coral Bleaching. *Human and Ecological Risk Assessment: An International Journal* **7**, 1271–1282 (2001).

29. S. De Mora, S. Demers, M. Vernet, *The Effects of UV Radiation in the Marine Environment* (Cambridge University Press, 2000).

30. R. A. Bone, D. W. Lee, J. M. Norman, Epidermal cells functioning as lenses in leaves of tropical rain-forest shade plants. *Appl. Opt.* **24**, 1408 (1985).

31. D. I. Speiser, D. J. Eernisse, S. Johnsen, A chiton uses aragonite lenses to form images. *Curr. Biol.* **21**, 665–670 (2011).

32. J. Aizenberg, A. Tkachenko, S. Weiner, L. Addadi, G. Hendler, Calcitic microlenses as part of the photoreceptor system in brittlestars. *Nature* **412**, 819–822 (2001).

33. K. M. Towe, Trilobite Eyes: Calcified Lenses in vivo. *Science* **179**, 1007–1009 (1973).

34. D. Gkikas, A. Argiropoulos, S. Rhizopoulou, Epidermal focusing of light and modelling of reflectance in floral-petals with conically shaped epidermal cells. *Flora - Morphology,*

Distribution, Functional Ecology of Plants **212**, 38–45 (2015).

35. H. L. Gorton, T. C. Vogelmann, Effects of Epidermal Cell Shape and Pigmentation on Optical Properties of Antirrhinum Petals at Visible and Ultraviolet Wavelengths. *Plant Physiol.* **112**, 879–888 (1996).

36. Q. O. N. Kay, H. S. Daoud, C. H. Stirton, Pigment distribution, light reflection and cell structure in petals. *Bot. J. Linn. Soc.* **83**, 57–83 (1981).

37. D. E. McCoy, *et al.*, Structurally assisted super black in colourful peacock spiders. *Proc. Biol. Sci.* **286**, 20190589 (2019).

38. M. R. Snow, A. Pring, P. Self, D. Losic, J. Shapter, The origin of the color of pearls in iridescence from nano-composite structures of the nacre. *Am. Mineral.* **89**, 1353–1358 (2004).

39. J. Salman, *et al.*, Hyperspectral interference tomography of nacre. *Proc. Natl. Acad. Sci. U. S. A.* **118** (2021).

40. W. L. Bragg, The refractive indices of calcite and aragonite. *Proceedings of the Royal Society of London. Series A, Containing Papers of a Mathematical and Physical Character* **105**, 370–386 (1924).

41. E. J. Weichel-Moore, R. J. Potter, Fibre Optical Properties of Ulexite. *Nature* **200**, 1163–1165 (1963).

42. Y. H. Ikuhara, S. Kondoh, K. Kikuta, S.-I. Hirano, Microstructure characterization of one-directionally oriented ulexite. *J. Mater. Res.* **13**, 778–783 (1998).

43. M. F. Land, Optics of the eyes ofPhronima and other deep-sea amphipods. *J. Comp. Physiol.* **145**, 209–226 (1981).

44. D.-E. Nilsson, The transparent compound eye ofHyperia (Crustacea): Examination with a new method for analysis of refractive index gradients. *J. Comp. Physiol.* **147**, 339–349 (1982).

45. J. Aizenberg, V. C. Sundar, A. D. Yablon, J. C. Weaver, G. Chen, Biological glass fibers: correlation between optical and structural properties. *Proc. Natl. Acad. Sci. U. S. A.* **101**, 3358–3363 (2004).

46. V. C. Sundar, A. D. Yablon, J. L. Grazul, M. Ilan, J. Aizenberg, Fibre-optical features of a glass sponge. *Nature* **424**, 899–900 (2003).

47. J. Aizenberg, *et al.*, Skeleton of Euplectella sp.: structural hierarchy from the nanoscale to the macroscale. *Science* **309**, 275–278 (2005).

48. R. Cattaneo-Vietti, *et al.*, Optical fibres in an Antarctic sponge. *Nature* **383**, 397–398 (1996).

49. B. Danis, A field guide to Antarctic sponges. *Project Implemented by SCAR-marBIN and ANTABIF. Available online at: http://afg. scarmarbin. be/guides/144164-a-field-guide-to-antarctic-sponges (accessed October 27, 2014)* (2013).

50. C. C. Perry, T. Keeling-Tucker, Biosilicification: the role of the organic matrix in structure control. *J. Biol. Inorg. Chem.* **5**, 537–550 (2000).

51. S. E. Beaulieu, Life on glass houses: sponge stalk communities in the deep sea. *Mar. Biol.* **138**, 803–817 (2001).

52. T. Saito, M. Takeda, Phylogeny of the family Spongicolidae (Crustacea: Stenopodidea): evolutionary trend from shallow-water free-living to deep-water sponge-associated habitat. *J. Mar. Biol. Assoc. U. K.* **83**, 119–131 (2003).

53. K. E. Carpenter, V. H. Niem, *The living marine resources of the Western Central Pacific: 1. Seaweeds, corals, bivalves and gastropods* (1998).

54. L. Li, C. Ortiz, Biological design for simultaneous optical transparency and mechanical robustness in the shell of Placuna placenta. *Adv. Mater.* **25**, 2344–2350 (2013).

55. J. G. Carter, G. R. Clark, Classification and phylogenetic significance of molluscan shell microstructure. *Series in Geology, Notes for Short Course* **13**, 50–71 (1985).

56. S. V. Popov, Formation of bivalve shells and their microstructure. *Paleontol. J.* **48**, 1519–1531 (2014).

57. E. Hecht, *Optics* (Pearson Education, Incorporated, 2017).

58. L. Li, *et al.*, Multifunctionality of chiton biomineralized armor with an integrated visual system. *Science* **350**, 952–956 (2015).

59. R. L. Pardy, Symbiotic algae and 14C incorporation in the freshwater clam, Anodonta. *Biol. Bull.* **158**, 349–355 (1980).

60. B. Morton, The biology, functional morphology and taxonomic status of Fluviolanatus Subtorta (Bivalvia: Trapeziidae), a heteromyarian bivalve possessing “Zooxanthellae.” *J. Malacol. Soc. Aust.* **5**, 113–140 (1982).

61. K. S. Naidu, G. R. South, Occurrence of an endozoic alga in the giant scallop Placopecten magellanicus (Gmelin). *Can. J. Zool.* **48**, 183–185 (1970).

62. M. C. Hartman, I. Pratt, Infection of the heart cockle, Clinocardium nuttallii, from Yaquina Bay, Oregon, with an endosymbiotic alga. *Journal of Invertebrate Pathology* **28**, 291–299 (1976).

63. D. S. Jones, D. K. Jacobs, Photosymbiosis in Clinocardium nuttalli: Implications for Tests of Photosymbiosis in Fossil Molluscs. *PALAIOS* **7**, 86 (1992).

64. K. Robson Brown, D. Bacheva, R. S. Trask, The structural efficiency of the sea sponge Euplectella aspergillum skeleton: bio-inspiration for 3D printed architectures. *J. R. Soc. Interface* **16**, 20180965 (2019).

65. A. E. Wetzel, *et al.*, Bioinspired Microstructured Polymer Surfaces with Antireflective Properties. *Nanomaterials (Basel)* **11** (2021).

66. C. Carteret, *et al.*, The vibrational spectrum of CaCO3 aragonite: a combined experimental and quantum-mechanical investigation. *J. Chem. Phys.* **138**, 014201 (2013).

67. Frech, Wang, Bates, The ir and Raman spectra of CaCO3 (aragonite). *Spectrochim. Acta A Mol. Biomol. Spectrosc.*

68. X. Song, Z. Liu, L. Wang, L. Song, Recent Advances of Shell Matrix Proteins and Cellular Orchestration in Marine Molluscan Shell Biomineralization. *Frontiers in Marine Science* **6** (2019).

69. J. A. Jones, *et al.*, Laser imaging polarimetry of nacre. *J. Biophotonics* **11**, e201800026 (2018).

70. D. E. McCoy, A. V. Shneidman, A. L. Davis, J. Aizenberg, Finite-difference Time-domain (FDTD) Optical Simulations: A Primer for the Life Sciences and Bio-Inspired Engineering. *Micron* **151**, 103160 (2021).

71. D. Chateigner, C. Hedegaard, H.-R. Wenk, Mollusc shell microstructures and crystallographic textures. *J. Struct. Geol.* **22**, 1723–1735 (2000).